

Kinetic based optimization enhanced by genetic dynamics

Giacomo Albi*, Federica Ferrarese[†] and Claudia Totzeck[‡]

Abstract

We propose and analyse a variant of the recently introduced kinetic based optimization method that incorporates ideas like survival-of-the-fittest and mutation strategies well-known from genetic algorithms. Thus, we provide a first attempt to reach out from the class of consensus/kinetic-based algorithms towards genetic metaheuristics. Different generations of genetic algorithms are represented via two species identified with different labels, binary interactions are prescribed on the particle level and then we derive a mean-field approximation in order to analyse the method in terms of convergence. Numerical results underline the feasibility of the approach and show in particular that the genetic dynamics allows to improve the efficiency, of this class of global optimization methods in terms of computational cost.

Keywords: global optimization, mean-field limit, Boltzmann equations, particle-based methods, consensus-based optimization.

Mathematics Subject Classification: 90C26, 90C56, 35Q93, 35Q20

1 Introduction

In recent years a new perspective on gradient-free methods for global optimization of non-convex high-dimensional functions was established. This arises from a new class of models which exploit collective dynamics of swarms and define communication strategies among the swarm members to find global optimizers, thereby allowing for rigorous convergence analysis using the mesoscopic approximations. In particular, the characterization of the long-time behaviour allows to prove that the swarms concentrate arbitrarily close by the unique global minimizer of the objective function, we refer to [25, 7, 14, 11, 12] and the overview in [28].

Similar to gradient-based methods [6], there are first-order and second-order models available, some of them including memory [14, 29] or momentum effects [9]. However, in

*Dipartimento di Informatica, Università di Verona, Verona, Italy, e-mail: giacomo.albi@univr.it

[†]Dipartimento di Matematica, Università di Trento, e-mail: federica.ferrarese@unitn.it

[‡]Department of Mathematics and Informatics, University of Wuppertal, e-mail: totzeck@uni-wuppertal.de

contrast to gradient-based methods as for example stochastic gradient descent, the landscape of the objective functions is explored via function evaluations only. In more detail, the objective value at the current position and the current position of the agents is exchanged, for example, with the help of a weighted mean value which is constructed such that the Laplace principle [10] applies. The dynamics is tailored such that the agents confine towards the weighted-mean on the one hand, and randomly explore the landscape on the other hand. This already indicates that the two components of the dynamics need to be well-balanced to obtain desirable results.

Consensus-based optimization (CBO) was a first step towards the mathematical understanding of metaheuristics for global optimization, such as particle swarm optimization (PSO) methods, where second order dynamics is used for the evolution of the particles [17, 26]. Recently, the gap between the first-order method CBO and PSO was bridged in [14], further extensions were provided for constrained optimization [5], and multi-objective problems [4, 18]. More recently, kinetic-based optimization (KBO) methods have been proposed in [3], where each agent with position x moves subject to the following interaction rules

$$x' = x + \nu_F(\hat{x}(t) - x) + \sigma_F D(x)\xi, \quad (1.1)$$

where x' denotes the post iteration position, σ_F , ν_F are positive parameters which allow to balance the exploitation and exploration of the swarm, ξ is a random perturbation term, $D(x)$ is a diffusion matrix and $\hat{x}(t)$ denotes the global estimate of the position of the global minimizer at time t . In addition to this dynamics a drift towards the local best and a local diffusion term is proposed in [3]. The corresponding dynamics is described by a multidimensional Boltzmann equation and can be simulated with the help of Monte Carlo algorithms [2, 24].

With this work, we aim at extending KBO algorithm reaching out towards genetic algorithms (GA) [20, 27], a very popular class of metaheuristics that is widely used in engineering. The GA models a natural selection process based on biological evolution [13, 21]. To this end, individuals (parents) from the current population are selected and their objective values (gene information) is combined to generate the next generation (children). The selection process is usually driven by a survival-of-the-fittest idea, hence over successive generations, the system is assumed to evolve towards an optimal solution. Agents in promising positions, i.e., with small objective values, are labeled as parents and the others are labeled as children. Leaders do not modify their position, hence they survive the iteration like in a survival-of-the-fittest strategy. In contrast, a child in position x interacts with a randomly chosen parent in position x_* and updates the position according to the rules

$$\begin{aligned} x' &= x_* && \text{with rate } \nu_F, \\ x' &= x && \text{with rate } 1 - \nu_F. \end{aligned} \quad (1.2)$$

Here x' denotes the post interaction position and $\nu_F > 0$ is the jump rate. Furthermore, mutations can occur, that means a child in position x encounters a random perturbation

of the form

$$x' = x + \sigma_F \xi, \quad (1.3)$$

where σ_F is a positive parameter and ξ random vector drawn from a normal distribution. Slight modifications of the mutation process can be considered, assuming that all children encounter a random perturbation of the type

$$x' = x + \sigma_F D(x) \xi, \quad (1.4)$$

with diffusion matrix $D(x)$.

Thus, to establish a relation between KBO and GA, we divide the swarm into two species called followers (children) and leaders (parents) via a labeling strategy, evolving according to different transition processes [1, 19].

More details are presented in the following section which are organized as follows: in Section 2 we introduce the Genetic Kinetic based optimization methods focusing on the description of the binary interactions rules which describes the dynamics. In Section 3, we derive the mean field, in particular the evolution equations of the density functions of the two species. In Section 2.2, we discuss different strategies of how to assign labels. In Section 4, we provide a theoretical analysis including the exponential decay of the variance and the convergence of the method to the global minimum. In Section 5, we describe Nanbu's algorithm which is used to obtain the numerical results presented in Section 6. Here, we show different numerical experiments, testing the efficiency in terms of success rate and number of iterations and compare the results of the GKBO algorithm, to KBO and genetic algorithms.

2 Genetic kinetic based optimization (GKBO)

The GKBO method we propose in the following enhances kinetic based optimization, which belongs to the class of consensus based algorithms, with ideas from genetic algorithms. To this end, we assume to have a population divided into two groups, similar to the parent and children populations in genetic algorithms. The two groups are specified with the help of labels leading to a modified KBO dynamic with followers and leaders. The dynamics is tailored in such a way that the the population clusters at the unique global minimum of the possibly non-convex objective function $\mathcal{E}: \mathbb{R}^d \rightarrow \mathbb{R}$. Hence, in the long time limit the dynamics solves the global optimization problem given by

$$\min_{x \in \mathbb{R}^d} \mathcal{E}(x), \quad (2.1)$$

where \mathcal{E} is assumed to have a unique global minimizer. In more detail, each agent is described by its position $x \in \mathbb{R}^d$ varying continuously and a binary variable for the leadership-level $\lambda \in \{0, 1\}$. In the following we identify leaders with $\lambda = 1$ and followers with $\lambda = 0$.

We are interested in the evolution of the density function

$$f = f(x, \lambda, t), \quad f : \mathbb{R}^d \times \{0, 1\} \times \mathbb{R}_+ \rightarrow \mathbb{R}_+ \quad (2.2)$$

where $t \in \mathbb{R}^+$ denotes as usual the time variable. In the rest of the paper we denote $f(x, \lambda, t)$ as $f_\lambda(x, t)$ and define

$$g(x, t) = \sum_{\lambda \in \{0, 1\}} f_\lambda(x, t), \quad (2.3)$$

to be the density of the whole population at time t . We assume that $g(x, t)$ is normalized, hence a probability measure and introduce the fractions $\rho_\lambda \in [0, 1]$ with $\lambda \in \{0, 1\}$ s.t. $\rho_0 + \rho_1 = 1$ and $f_\lambda(x, t)/\rho_\lambda$ are probability measures as well.

2.1 Binary interaction between agents

A binary interaction of agents with state (x, λ) and (x_*, λ_*) is described by their post-interaction positions given by

$$\begin{aligned} x' &= x + (\nu_F(x_* - x) + \sigma_F D(x)\xi) \lambda_* (1 - \lambda) + \nu_L(\hat{x}(t) - x)\lambda, \\ x'_* &= x_*, \end{aligned} \quad (2.4)$$

where σ_F, ν_F, ν_L , are positive parameters, ξ is a normally distributed random number and $D(x)$ is the diffusion matrix, defined to be either

$$D(x) = |\hat{x}(t) - x| Id_d, \quad (2.5)$$

in the case of isotropic diffusion[25], or

$$D(x) = \text{diag}\{(\hat{x}(t) - x)_1, \dots, (\hat{x}(t) - x)_d\}, \quad (2.6)$$

in the case of anisotropic diffusion, [8]. In equation (2.5)-(2.6) the term $\hat{x}(t)$ is the global estimate of the best position of the minimizer. The term $\hat{x}(t)$ is computed as a convex combination of particle locations weighted by the cost function according to Laplace principle ([10]). In case we consider the whole population, we have

$$\hat{x}(t) = \frac{\int_{\mathbb{R}^d} x e^{-\alpha \mathcal{E}(x)} g(x, t) dx}{\int_{\mathbb{R}^d} e^{-\alpha \mathcal{E}(x)} g(x, t) dx}, \quad (2.7)$$

and Laplace principle yields

$$\lim_{\alpha \rightarrow \infty} \left(-\frac{1}{\alpha} \int_{\mathbb{R}^d} e^{-\alpha \mathcal{E}(x)} g(x, t) dx \right) = \inf_{x \in \text{supp } g(x, t)} \mathcal{E}(x). \quad (2.8)$$

In the section on numerical results we will also consider variants, where the weighted mean is computed with information of leaders or followers only.

Remark 1. Note that (2.4) implies that no follower-follower interactions are considered, since if both λ and λ_* are equal to zero the agents keep their positions.

2.2 Emergence of leaders and followers

The emergence of leaders and followers is realized with the help of a transition operator which acts as follows

$$\begin{aligned}\mathcal{T}[f_0](x, t) &= \pi_{L \rightarrow F}(x, \lambda; f) f_1(x, t) - \pi_{F \rightarrow L}(x, \lambda; f) f_0(x, t), \\ \mathcal{T}[f_1](x, t) &= \pi_{F \rightarrow L}(x, \lambda; f) f_0(x, t) - \pi_{L \rightarrow F}(x, \lambda; f) f_1(x, t),\end{aligned}\tag{2.9}$$

where $\pi_{F \rightarrow L}(\cdot)$ and $\pi_{L \rightarrow F}(\cdot)$ are certain transition rates, possibly depending on the current states. In the simplest case, if we assume that leaders emerge with fixed rate $\pi_{FL} > 0$ and return to the followers status with fixed rate $\pi_{LF} > 0$ then the transition rates reduce to

$$\pi_{L \rightarrow F} = \pi_{LF}, \quad \pi_{F \rightarrow L} = \pi_{FL}.\tag{2.10}$$

However, we also cover more general cases, as for example proposed in [15], where each agent in position x is associated with a weight

$$\begin{aligned}\omega(x, t) &= \frac{1}{N} \# \{y \in \mathcal{A}(t) : |\mathcal{E}(x_{min}) - \mathcal{E}(y)| < |\mathcal{E}(x_{min}) - \mathcal{E}(x)|\} \\ &= \frac{1}{N} \sum_{\lambda \in \{0,1\}} \int_{\mathbb{R}^d} \chi_{[0,1]} \left(\frac{|\mathcal{E}(x_{min}(t)) - \mathcal{E}(y)|}{|\mathcal{E}(x_{min}(t)) - \mathcal{E}(x)|} \right) f(y, \lambda, t) dy,\end{aligned}\tag{2.11}$$

with $\chi_{[0,1]}(\cdot)$ denoting the characteristic function of the interval $[0, 1)$ and

$$x_{min}(t) = \arg \min_{x \in \mathcal{A}(t)} \mathcal{E}(x),\tag{2.12}$$

where $\mathcal{A}(t)$ is the set of agents at time t . Assuming that agents with weight smaller than a certain threshold $\bar{\omega}$, which depends on the amount of leaders that we would like to generate, are in the leaders status while the others are in the followers status, then we can write the transition rates as follows

$$\pi_{L \rightarrow F} = \begin{cases} 1, & \text{if } \omega(x, t) > \bar{\omega}, \\ 0, & \text{if } \omega(x, t) \leq \bar{\omega}, \end{cases} \quad \pi_{F \rightarrow L} = \begin{cases} 0, & \text{if } \omega(x, t) \geq \bar{\omega}, \\ 1, & \text{if } \omega(x, t) < \bar{\omega}. \end{cases}\tag{2.13}$$

The evolution of the emergence and decay of leaders can be described by the master equation

$$\frac{d}{dt} \rho_\lambda(t) + \int_{\mathbb{R}^{2d}} \mathcal{T}[f](x, \lambda, t) dx = 0,\tag{2.14}$$

for $\lambda \in \{0, 1\}$, with $\rho_\lambda(t) = \int_{\mathbb{R}^d} f_\lambda(x, t) dx$. From the above definition of the transition operator $\mathcal{T}[\cdot]$, it follows that

$$\frac{d}{dt} \sum_{\lambda \in \{0,1\}} \rho_\lambda(t) = 0.\tag{2.15}$$

In case of constant transition rates

$$\pi_{L \rightarrow F}(\cdot) = \pi_{LF}, \quad \pi_{F \rightarrow L}(\cdot) = \pi_{FL}, \quad (2.16)$$

we can rewrite equation (2.14) as

$$\begin{cases} \partial_t \rho_1(t) = \pi_{FL} \rho_0(t) - \pi_{LF} \rho_1(t), \\ \partial_t \rho_0(t) = \pi_{LF} \rho_1(t) - \pi_{FL} \rho_0(t). \end{cases} \quad (2.17)$$

which allows us to calculate its stationary solution explicitly as

$$\rho_1^\infty = \frac{\pi_{FL}}{\pi_{LF} + \pi_{FL}}, \quad \rho_0^\infty = \frac{\pi_{LF}}{\pi_{LF} + \pi_{FL}}. \quad (2.18)$$

Remark 2. The weighted strategy is inspired from the selection criterion of GA, where parents are chosen to be the agents in best position w.r.t. the cost function. In the numerical experiments we will also consider a mixed strategy, assuming that a certain percentage \bar{p} of the total amount of leaders change their label according to the weighted strategy and the remaining ones changes their label randomly.

3 Derivation of the mean-field equation

Combining the interaction and transition dynamic described in the previous section, we obtain the evolution of the density function $f_\lambda(x, t)$ which is described by the integro-differential equation of Boltzmann-type

$$\partial_t f_\lambda(x, t) - \mathcal{T}[f_\lambda](x, t) = \sum_{\lambda_* \in \{0,1\}} Q(f_\lambda, f_{\lambda_*})(x, t), \quad (3.1)$$

where $\mathcal{T}[\cdot]$ is the transition operator and $Q(\cdot, \cdot)$ is the binary interaction operator defined as follows

$$Q(f_\lambda, f_{\lambda_*}) = \eta \int_{\mathbb{R}^{2d}} \left(\frac{1}{J} f_\lambda(x', t) f_{\lambda_*}(x'_*, t) - f_\lambda(x, t) f_{\lambda_*}(x_*, t) \right) dx dx_*, \quad (3.2)$$

where (x', x'_*) are the pre-interaction positions generated by the couple (x, x_*) after the interaction (2.4). The term J denotes the Jacobian of the transformation $(x, x_*) \rightarrow (x', x'_*)$ and $\eta > 0$ is a constant relaxation rate representing the interaction frequency. To obtain a weak-formulation, we consider a test function $\phi(x)$ and rewrite the collision operator

$$\int_{\mathbb{R}^d} Q(f_\lambda, f_{\lambda_*})(x, t) \phi(x) dx = \eta \int_{\mathbb{R}^{2d}} (\phi(x') - \phi(x)) f_{\lambda_*}(x_*, t) f_\lambda(x, t) dx dx_*. \quad (3.3)$$

Hence, the weak form of (3.1) reads

$$\begin{aligned} \frac{\partial}{\partial t} \int_{\mathbb{R}^d} f_\lambda(x, t) \phi(x) dx - \int_{\mathbb{R}^d} \mathcal{T}[f_\lambda](x, t) \phi(x) dx = \\ \eta \sum_{\lambda_* \in \{0, 1\}} \left\langle \int_{\mathbb{R}^{2d}} [\phi(x') - \phi(x)] f_\lambda(x, t) f_{\lambda_*}(x_*, t) dx dx_* \right\rangle. \end{aligned} \quad (3.4)$$

To simplify the computations, we assume to have constant transition rates (2.16) and to be in the quasi-stationary state ρ_λ^∞ i.e. $\rho_\lambda \approx \rho_\lambda^\infty$ for any $\lambda \in \{0, 1\}$ as in (2.18). Moreover, we introduce the scaling parameter $\varepsilon > 0$ and consider

$$\nu_F \rightarrow \frac{\nu_F}{\rho_1} \varepsilon, \quad \nu_L \rightarrow \frac{\nu_L}{\rho_1} \varepsilon, \quad \sigma_F \rightarrow \frac{\sigma_F}{\sqrt{\rho_1}} \sqrt{\varepsilon}, \quad \eta \rightarrow \frac{1}{\varepsilon}. \quad (3.5)$$

This scaling corresponds to the case where the interaction kernel concentrates on binary interactions producing very small changes in the agents position but at the same time the number of interactions becomes very large.

To obtain the mean-field equation, we consider the Taylor expansion of the test function $\phi(x')$ centred in x given by

$$\phi(x') - \phi(x) = \nabla_x \phi(x) \cdot (x' - x) + \frac{1}{2} \Delta_x \phi(x) (x' - x)^2 + \mathcal{O}(\varepsilon^2), \quad (3.6)$$

and use it to rewrite (3.4) as follows

$$\begin{aligned} \frac{\partial}{\partial t} \int_{\mathbb{R}^d} f_\lambda(x, t) \phi(x) dx - \int_{\mathbb{R}^d} \mathcal{T}[f_\lambda](x, t) \phi(x) dx = \\ \sum_{\lambda_* \in \{0, 1\}} \left\{ \int_{\mathbb{R}^{2d}} \left(\frac{\nu_F}{\rho_1} (x_* - x) \lambda_* (1 - \lambda) + \frac{\nu_L}{\rho_1} (\hat{x}(t) - x) \lambda \right) \cdot \nabla_x \phi(x) df_\lambda df_{\lambda_*} \right. \\ \left. + \frac{\sigma_F^2}{2} \int_{\mathbb{R}^{2d}} D^2(x) (1 - \lambda)^2 \lambda_*^2 \Delta_x \phi(x) df_\lambda df_{\lambda_*} \right\} + \mathcal{O}(\varepsilon), \end{aligned} \quad (3.7)$$

where for simplicity we write $df_\lambda = f_\lambda(x, t) dx$ and $df_{\lambda_*} = f_{\lambda_*}(x_*, t) dx_*$. Now, taking the limit $\varepsilon \rightarrow 0$, integrating by parts and rewriting the equation in strong form yields

$$\begin{aligned} \frac{\partial}{\partial t} f_0(x, t) - \mathcal{T}[f_0](x, t) &= \frac{\sigma_F^2}{2} \Delta_x [D^2(x) f_0(x, t)] - \nu_F \nabla_x \cdot \left[\left(\frac{m_1(t)}{\rho_1} - x \right) f_0(x, t) \right], \\ \frac{\partial}{\partial t} f_1(x, t) - \mathcal{T}[f_1](x, t) &= -\frac{\nu_L}{\rho_1} \nabla_x \cdot \left[(\hat{x}(t) - x) f_1(x, t) \right], \end{aligned} \quad (3.8)$$

where $D(x)$ is the diffusion matrix defined in (2.6)-(2.5), $\hat{x}(t)$ is the global estimate of the global minimizer at time t defined in equation (2.7) and

$$m_1(t) = \int_{\mathbb{R}^{2d}} x f_1(x, t) dx \quad (3.9)$$

denotes the centre of mass of the leaders at time t .

Remark 3. Multiplying both side of the second equation in (3.8) by x/ν_L integrating and taking the formal limit $\nu_L \rightarrow +\infty$, we get

$$\frac{m_1(t)}{\rho_1} = \hat{x}(t).$$

Plugging it into the first equation in (3.8), assuming $\mathcal{T}[f_0](x, t) = 0$, we recover the equation that governs the dynamics in absence of leaders that is

$$\frac{\partial}{\partial t} f_0(x, t) = \frac{\sigma_F^2}{2} \Delta_x [D(x)^2 f_0(x, t)] + \nu_F \nabla_x \cdot [(\hat{x}(t) - x) f_0(x, t)]. \quad (3.10)$$

To summarize, the diagram in Figure 1 describes the relation between the three algorithms at the particle and mean field level.

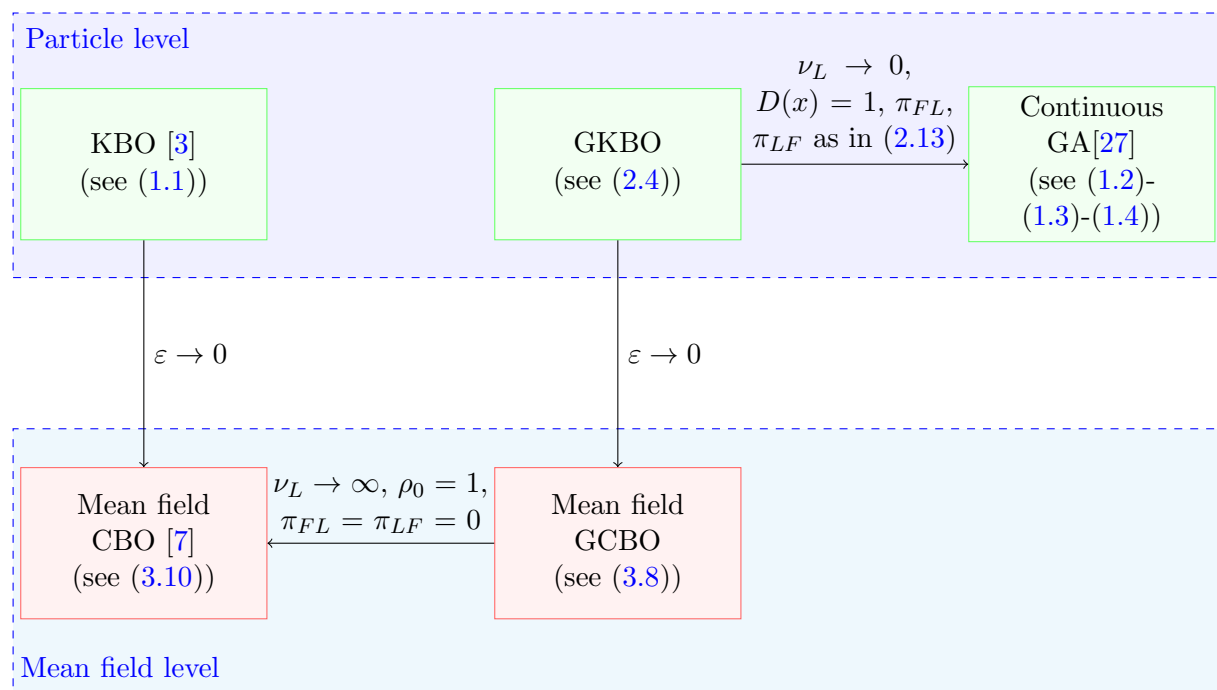


Figure 1: Diagram describing the relation between the KBO, the GKBO with weighted and random strategies and the GA.

4 Moments estimates and convergence to the global minimum

Following the idea introduced in [3, 25] we provide moments estimates, showing that the variance decreases exponentially to zero, and we prove the convergence of the method toward the position of the global minimum. In this section we study the behaviour of the two population dynamic, we therefore assume throughout this section $\rho_0, \rho_1 > 0$.

4.1 Evolution of the moment estimates

We define the first two moments of the total population by

$$m(t) = m_0(t) + m_1(t), \quad e(t) = e_0(t) + e_1(t), \quad (4.1)$$

respectively, where

$$\begin{aligned} m_0(t) &= \int_{\mathbb{R}^d} x f_0(x, t) dx, & e_0(t) &= \int_{\mathbb{R}^d} |x|^2 f_0(x, t) dx, \\ m_1(t) &= \int_{\mathbb{R}^d} x f_1(x, t) dx, & e_1(t) &= \int_{\mathbb{R}^d} |x|^2 f_1(x, t) dx, \end{aligned} \quad (4.2)$$

are the first two moments of the subpopulations $f_\lambda(x, t)$ for $\lambda \in \{0, 1\}$ and

$$V(t) = v_0(t) + v_1(t), \quad (4.3)$$

the sum of the variances of the subpopulations given by

$$v_0(t) = \int_{\mathbb{R}^d} \left| x - \frac{m_0}{\rho_0} \right|^2 f_0(x, t) dx, \quad v_1(t) = \int_{\mathbb{R}^d} \left| x - \frac{m_1}{\rho_1} \right|^2 f_1(x, t) dx. \quad (4.4)$$

Remark 4. For the following computations it is helpful to have in mind that

$$m(t) = \int_{\mathbb{R}^d} x(f_0(x, t) + f_1(x, t)) dx, \quad e(t) = \int_{\mathbb{R}^d} |x|^2 (f_0(x, t) + f_1(x, t)) dx,$$

but due to the nonlinearity

$$V(t) \neq \int_{\mathbb{R}^d} |x - m(t)|^2 (f_0(x, t) + f_1(x, t)) dx.$$

Proposition 1. *Let us assume the transitions have equilibrated, that is, $\rho_0 \equiv \rho_0^\infty$ and $\rho_1 \equiv \rho_1^\infty$. Furthermore let $\mathcal{E}(x)$ positive and bounded for all $x \in \mathbb{R}^d$, in particular, there exist constants $\underline{\mathcal{E}}, \bar{\mathcal{E}} > 0$ such that*

$$\underline{\mathcal{E}} := \inf_x \mathcal{E}(x) \leq \mathcal{E}(x) \leq \sup_x \mathcal{E}(x) := \bar{\mathcal{E}}, \quad (4.5)$$

and define $\tilde{\sigma} = k\sigma_F^2 b_{\underline{\mathcal{E}}}$, with $b_{\underline{\mathcal{E}}} = \exp(\alpha(\bar{\mathcal{E}} - \underline{\mathcal{E}}))$, where $k = d$ in the case of isotropic diffusion and $k = 1$ in the case of anisotropic diffusion. If

$$\nu_F = \nu_L, \quad \nu_F > \max \left\{ \frac{\tilde{\sigma}}{2}, \frac{\rho_1}{2} \right\}, \quad (4.6)$$

it holds

$$\begin{aligned} \frac{d}{dt}m(t) &= \nu_F(\hat{x} - m)(t), \\ \frac{d}{dt}V(t) &\leq (-2\nu_F + \tilde{\sigma})V(t) + (\tilde{\sigma}\rho_0\rho_1 - \pi_{LF}\rho_1 - \pi_{FL}\rho_0) \left(\frac{m_0(t)}{\rho_0} - \frac{m_1(t)}{\rho_1} \right)^2. \end{aligned} \quad (4.7)$$

Proof. Let us define for simplicity

$$\begin{aligned} M_\lambda(t) &= \frac{1}{\rho_\lambda} \int_{\mathbb{R}^d} x f_\lambda(x, t) dx, & E_\lambda(t) &= \frac{1}{\rho_\lambda} \int_{\mathbb{R}^d} |x|^2 f_\lambda(x, t) dx, \\ V_\lambda(t) &= \frac{1}{\rho_\lambda} \int_{\mathbb{R}^d} |x - M_\lambda|^2 f_\lambda(x, t) dx, \end{aligned} \quad (4.8)$$

for any $\lambda \in \{0, 1\}$ such that

$$\begin{aligned} m(t) &= \rho_0 M_0(t) + \rho_1 M_1(t), & e(t) &= \rho_0 E_0(t) + \rho_1 E_1(t), \\ V(t) &= \rho_0 V_0(t) + \rho_1 V_1(t). \end{aligned} \quad (4.9)$$

We begin by computing the evolution of the first moments

$$\frac{d}{dt}m(t) = \rho_0 \frac{d}{dt}M_0(t) + \rho_1 \frac{d}{dt}M_1(t). \quad (4.10)$$

For the first term of (4.10) we obtain

$$\begin{aligned} \rho_0 \frac{d}{dt}M_0(t) &= \int_{\mathbb{R}^d} x \partial_t f_0 = \\ &= \int_{\mathbb{R}^d} x \left[-\pi_{LF} f_1 + \pi_{FL} f_0 + \right. \\ &\quad \left. - \nabla_x \cdot (\nu_F(M_1 - x)f_0) + \frac{\sigma_F^2}{2} \Delta_x (D^2(x)f_0) \right] dx = \\ &= -\pi_{LF}\rho_1 M_1(t) + \pi_{FL}\rho_0 M_0(t) + \rho_0 \nu_F (M_1 - M_0)(t). \end{aligned} \quad (4.11)$$

and for the second term in (4.10) it holds

$$\begin{aligned} \rho_1 \frac{d}{dt}M_1(t) &= \int_{\mathbb{R}^d} x \partial_t f_1 = \\ &= \int_{\mathbb{R}^d} x \left[\pi_{LF} f_1 - \pi_{FL} f_0 - \nabla_x \cdot \left(\frac{\nu_L}{\rho_1} (\hat{x} - x) f_1 \right) \right] dx = \\ &= \pi_{LF}\rho_1 M_1(t) - \pi_{FL}\rho_0 M_0(t) + \nu_L (\hat{x} - M_1)(t). \end{aligned} \quad (4.12)$$

Together this yields

$$\frac{d}{dt}m(t) = \nu_F \rho_0 (M_1 - M_0)(t) + \nu_L (\hat{x} - M_1)(t), \quad (4.13)$$

and recalling the definition of $M_0(t)$ and $M_1(t)$ in (4.8) we get

$$\frac{d}{dt}m(t) = \nu_L \hat{x}(t) - \nu_F m(t) + \left(\nu_F \frac{\rho_0}{\rho_1} + \nu_F - \frac{\nu_L}{\rho_1} \right) m_1(t). \quad (4.14)$$

By the first assumption in (4.6) we can recover the first equation of the statement.

For $V(t)$ we have

$$\frac{d}{dt}V(t) = \rho_0 \frac{d}{dt}V_0(t) + \rho_1 \frac{d}{dt}V_1(t). \quad (4.15)$$

We investigate the terms separately. First, we obtain

$$\begin{aligned} \frac{d}{dt}V_0(t) &= \frac{1}{\rho_0} \frac{d}{dt} \int_{\mathbb{R}^d} |x - M_0(t)|^2 df_0 = \\ &= \underbrace{\frac{2}{\rho_0} \int_{\mathbb{R}^d} \left(x - M_0(t), -\frac{d}{dt}M_0(t) \right) df_0}_{=: I_0} + \underbrace{\frac{1}{\rho_0} \int_{\mathbb{R}^d} |x - M_0(t)|^2 \partial_t f_0}_{=: I_1}. \end{aligned} \quad (4.16)$$

We note that I_0 vanishes, since $2\rho_0^{-1} \int_{\mathbb{R}^d} x - M_0(t) df_0 = 0$. We divide I_1 into its drift, diffusion and transition parts to obtain

$$I_1 =: I_1^0 + I_1^1 + I_1^2, \quad (4.17)$$

with

$$\begin{aligned} I_1^0 &= \frac{1}{\rho_0} \int_{\mathbb{R}^d} |x - M_0(t)|^2 (-\nu_F \nabla_x \cdot ((M_1(t) - x) f_0)) dx = \\ &= \frac{2\nu_F}{\rho_0} \int_{\mathbb{R}^d} (x - M_0(t))(M_1(t) - x) df_0 = \\ &= 2\nu_F (M_0(t)M_1(t) - E_0(t) - M_0(t)M_1(t) + M_0^2(t)) = -2\nu_F V_0, \end{aligned} \quad (4.18)$$

and, by an application of Jensen inequality we get

$$\begin{aligned}
I_1^1 &= \frac{1}{\rho_0} \int_{\mathbb{R}^d} |x - M_0(t)|^2 \Delta_x \left(\frac{\sigma_F^2}{2} D^2(x) f_0 \right) dx = \\
&= \frac{\sigma_F^2}{2\rho_0} \int_{\mathbb{R}^d} k |\hat{x}(t) - x|^2 df_0 = \\
&= \frac{\sigma_F^2}{2\rho_0} \int_{\mathbb{R}^d} k \int_{\mathbb{R}^d} \left| \frac{\int_{\mathbb{R}^d} (y-x) e^{-\alpha \mathcal{E}(y)} g(y) dy}{\int_{\mathbb{R}^d} e^{-\alpha \mathcal{E}(y)} g(y) dy} \right|^2 df_0 = \\
&\leq \frac{\tilde{\sigma}}{\rho_0} \int_{\mathbb{R}^{2d}} |y-x|^2 g(y) f_0(x) dx dy = \\
&= \frac{\tilde{\sigma}}{\rho_0} (\rho_0 E_0(t) + \rho_1 E_1(t) - (\rho_0 M_0(t) + \rho_1 M_1(t))^2) = \\
&= \frac{\tilde{\sigma}}{\rho_0} \left(V(t) + \rho_0 \rho_1 (M_0(t) - M_1(t))^2 \right),
\end{aligned} \tag{4.19}$$

and finally,

$$\begin{aligned}
I_1^2 &= \frac{1}{\rho_0} \int_{\mathbb{R}^d} |x - M_0(t)|^2 (-\pi_{LF} f_1 + \pi_{FL} f_0) dx = \\
&\quad - \frac{\pi_{LF}}{\rho_0} \int_{\mathbb{R}^d} (x^2 + M_0^2(t) - 2xM_0(t)) df_1 + \pi_{FL} V_0(t) = \\
&\quad - \frac{\pi_{LF}}{\rho_0} (\rho_1 V_1(t) + \rho_1 (M_0 - M_1)^2(t)) + \pi_{FL} V_0(t),
\end{aligned} \tag{4.20}$$

where we add and subtract $\rho_1 M_1^2(t)$ in the last term of I_1^2 .

For $V_1(t)$ we have

$$\begin{aligned}
\frac{d}{dt} V_1(t) &= \frac{1}{\rho_1} \frac{d}{dt} \int_{\mathbb{R}^d} |x - M_1(t)|^2 df_1 = \\
&\quad \underbrace{\frac{2}{\rho_1} \int_{\mathbb{R}^d} \left(x - M_1(t), -\frac{d}{dt} M_1(t) \right) df_0}_{=: I_2} + \underbrace{\frac{1}{\rho_1} \int_{\mathbb{R}^d} |x - M_1(t)|^2 \partial_t f_1}_{=: I_3}.
\end{aligned} \tag{4.21}$$

Similarly to the case I_0 one can easily conclude that I_2 vanishes. We divide I_3 into the drift and transition part to obtain

$$I_3 = I_3^0 + I_3^1, \tag{4.22}$$

with

$$\begin{aligned}
I_3^0 &= \frac{1}{\rho_1} \int_{\mathbb{R}^d} |x - M_1(t)|^2 \left(-\frac{\nu_L}{\rho_1} \nabla_x \cdot ((\hat{x}(t) - x) f_1) \right) dx = \\
&= \frac{2\nu_L}{\rho_1^2} \int_{\mathbb{R}^d} (x - M_1(t)) (\hat{x}(t) - x) df_1 = \\
&= \frac{2\nu_L}{\rho_1} (M_1(t) \hat{x}(t) - E_1(t) - M_1(t) \hat{x}(t) + M_1^2(t)) = -2 \frac{\nu_L}{\rho_1} V_1,
\end{aligned} \tag{4.23}$$

and

$$\begin{aligned}
I_3^2 &= \frac{1}{\rho_1} \int_{\mathbb{R}^d} |x - M_1(t)|^2 (\pi_{LF} f_1 - \pi_{FL} f_0) dx = \\
&= -\frac{\pi_{FL}}{\rho_1} \int_{\mathbb{R}^d} (x^2 + M_1^2(t) - 2xM_1(t)) df_0 + \pi_{LF} V_1(t) = \\
&= -\frac{\pi_{FL}}{\rho_1} (\rho_0 V_0(t) + \rho_0 (M_0 - M_1)^2(t)) + \pi_{LF} V_1(t),
\end{aligned} \tag{4.24}$$

where we add and subtract $\rho_0 M_0^2(t)$ in the last term of I_3^2 .

Altogether, we get

$$\begin{aligned}
\frac{d}{dt} V(t) &\leq \rho_1 \left(2\nu_F + \rho_0 - \frac{2\nu_F}{\rho_1} \right) V_0(t) + (-2\nu_F + \tilde{\sigma}) V(t) + \\
&\quad + (\tilde{\sigma} \rho_0 \rho_1 - \pi_{LF} \rho_1 - \pi_{FL} \rho_0) (M_0 - M_1)^2(t).
\end{aligned} \tag{4.25}$$

Using the assumptions, we recover the second inequality in (4.7). \square

Corollary 1. Let the assumptions of Proposition 1 hold, and in addition suppose that

$$\nu_F > \max \left\{ \frac{\pi_{LF} \rho_1}{\rho_0 (1 - b_{\bar{\mathcal{E}}} \rho_1)}, \frac{\pi_{FL}}{b_{\bar{\mathcal{E}}} \rho_0} \right\}, \quad \text{with } b_{\bar{\mathcal{E}}} = e^{\alpha(\underline{\mathcal{E}} - \bar{\mathcal{E}})}. \tag{4.26}$$

Then it holds

$$\left| \frac{m_0(t)}{\rho_0} - \frac{m_1(t)}{\rho_1} \right|^2 \rightarrow 0, \quad V(t) \rightarrow 0, \quad \text{as } t \rightarrow \infty. \tag{4.27}$$

Proof. Let us first study the behavior of $|M_0 - M_1|^2(t)$. We have

$$\begin{aligned}
\frac{d}{dt} |M_0 - M_1|^2(t) &= 2(M_0 - M_1)(t) \frac{d}{dt} (M_0 - M_1)(t) \\
&\leq -2\nu_F |M_0 - M_1|^2(t) + 2(M_0 - M_1)(t) (\mathcal{C}_1 M_1(t) - \mathcal{C}_0 M_0(t)) \\
&= -2\nu_F |M_0 - M_1|^2(t) - 2 \begin{bmatrix} M_0(t) \\ M_1(t) \end{bmatrix}^T \begin{bmatrix} \mathcal{C}_0 & -\mathcal{C}_0 \\ -\mathcal{C}_1 & \mathcal{C}_1 \end{bmatrix} \begin{bmatrix} M_0(t) \\ M_1(t) \end{bmatrix},
\end{aligned} \tag{4.28}$$

with

$$\mathcal{C}_0 = -\frac{\pi_{FL} - \nu_F \rho_0 b_{\bar{\mathcal{E}}}}{\rho_1}, \quad \mathcal{C}_1 = \frac{-\pi_{LF} \rho_1 + \nu_F \rho_0 (1 - \rho_1 b_{\bar{\mathcal{E}}})}{\rho_0 \rho_1}, \tag{4.29}$$

and we used equations (4.11)-(4.12) and the estimate

$$\hat{x}(t) = \frac{\int_{\mathbb{R}^d} x e^{-\alpha \mathcal{E}(x)} g(x, t) dx}{\int_{\mathbb{R}^d} e^{-\alpha \mathcal{E}(x)} g(x, t) dx} \geq \frac{e^{\alpha \underline{\mathcal{E}}}}{e^{\alpha \bar{\mathcal{E}}}} \int_{\mathbb{R}^d} x g(x, t) dx := b_{\bar{\mathcal{E}}} m(t). \tag{4.30}$$

Note that, if condition (4.26) holds then $\mathcal{C}_0, \mathcal{C}_1 > 0$ and so

$$-2 \begin{bmatrix} M_0(t) \\ M_1(t) \end{bmatrix}^T \begin{bmatrix} \mathcal{C}_0 & -\mathcal{C}_0 \\ -\mathcal{C}_1 & \mathcal{C}_1 \end{bmatrix} \begin{bmatrix} M_0(t) \\ M_1(t) \end{bmatrix} \leq 0, \quad (4.31)$$

since the above matrix is weakly diagonal dominant and hence positive semidefinite. Altogether, we obtain the estimate

$$\frac{d}{dt} |M_0 - M_1|^2(t) \leq -2\nu_F |M_0 - M_1|^2(t). \quad (4.32)$$

and an application of Grönwall lemma yields

$$|M_0 - M_1|^2(t) \leq |M_0 - M_1|^2(0) e^{-2\nu_F t}, \quad (4.33)$$

which allow us to conclude $|M_0 - M_1|^2(t) \rightarrow 0$ as $t \rightarrow \infty$.

In particular, this implies

$$|M_0 - M_1|^2(t) \leq |M_0 - M_1|^2(0), \quad (4.34)$$

which helps us to show the second statment. Indeed, we rewrite the second inequality in (4.7) in integral form as

$$V(t) \leq V(0) + \mathcal{C}_v^0 |M_0 - M_1|^2(0) \int_0^t ds - \mathcal{C}_v \int_0^t V(s) ds, \quad (4.35)$$

with $\mathcal{C}_v^0 = \tilde{\sigma} \rho_0 \rho_1 - \pi_{LF} \rho_1 - \pi_{FL} \rho_0$ and $\mathcal{C}_v = 2\nu_F - \tilde{\sigma}$. Moreover, we note that

$$t \rightarrow V(0) + \mathcal{C}_v^0 |M_0 - M_1|^2(0) t,$$

is a non-decreasing function. Hence, again using Grönwall lemma, we get

$$V(t) \leq \left[V(0) + \mathcal{C}_v^0 |M_0 - M_1|^2(0) t \right] e^{-\mathcal{C}_v t}, \quad (4.36)$$

which implies $V(t) \rightarrow 0$ as $t \rightarrow \infty$. □

The fact that $V(t)$ vanishes in the limit $t \rightarrow \infty$ allows us to conclude that the crowd concentrates. However, the position of the concentration point is unknown. This position is quantified in the following section.

4.2 Convergence to the global minimum

In this section, we determine the conditions under which the mean value of the population is a reasonable approximation of the global minimizer.

Proposition 2. *Suppose the assumptions of Proposition 1 hold. Further, we assume that $\mathcal{E} \in C^2(\mathbb{R}^d)$ and that there exist constants $c_1, c_2 > 0$ such that*

$$\sup_{y \in \mathbb{R}^2} |\nabla \mathcal{E}(y)| \leq c_1, \quad \sup_{y \in \mathbb{R}^2} |\Delta \mathcal{E}(y)| \leq c_2, \quad (4.37)$$

and that the initial condition is well-prepared in the sense that the minimizer of \mathcal{E} is in the support of the initial population and

$$\frac{\mu}{M_\alpha^2(0)} \leq \frac{3}{4}, \quad (4.38)$$

is satisfied with

$$M_\alpha(t) = \int_{\mathbb{R}^d} e^{-\alpha \mathcal{E}(x)} g(x) dx, \quad (4.39)$$

and

$$\begin{aligned} \mu = 2\alpha e^{-\alpha \underline{\mathcal{E}}} & \left[c_1 \sqrt{2} \left(\nu_F + \frac{\nu_F}{\rho_1} \right) + c_2 \sigma_F^2 k \right] \cdot \\ & \cdot \left[\max \left\{ \frac{1}{\mathcal{C}_v} V(0) + \gamma_m \left(\frac{\mathcal{C}_v^0}{\mathcal{C}_v^2} + \frac{\rho_0 \rho_1}{2\nu_F} \right), \frac{2}{\mathcal{C}_v} V(0) + \frac{4\mathcal{C}^*}{\mathcal{C}_v} + \frac{\sqrt{\rho_0 \rho_1 \gamma_m}}{\nu_F} \right\} \right], \end{aligned} \quad (4.40)$$

with

$$\mathcal{C}_v^0 = \tilde{\sigma} \rho_0 \rho_1 - \pi_{LF} \rho_1 - \pi_{FL} \rho_0, \quad \mathcal{C}_v = 2\nu_F - \tilde{\sigma}, \quad \gamma_m = \left(\frac{m_0(0)}{\rho_0} - \frac{m_1(0)}{\rho_1} \right)^2,$$

and \mathcal{C}^* is the maximal value of

$$t \rightarrow e^{-\frac{\mathcal{C}_v}{4} t} \sqrt{\mathcal{C}_v^0 \gamma_m t}.$$

Then there exists $\tilde{x} \in \mathbb{R}^d$ such that $m(t) \rightarrow \tilde{x}$ as $t \rightarrow \infty$ and

$$\mathcal{E}(\tilde{x}) = \underline{\mathcal{E}} + r(\alpha) + \frac{\log 2}{\alpha}, \quad (4.41)$$

where $r(\alpha) = -\frac{1}{\alpha} \log(M_\alpha(0)) - \underline{\mathcal{E}} \rightarrow 0$, as $\alpha \rightarrow \infty$.

Proof. First, we show

$$\left| \frac{d}{dt} m(t) \right| \rightarrow 0, \quad (4.42)$$

as $t \rightarrow \infty$. To this end, we rewrite

$$\left| \frac{d}{dt} m(t) \right| = \left| \nu_F \int_{\mathbb{R}^d} \left(\frac{e^{-\alpha \mathcal{E}(x)}}{M_\alpha(t)} - 1 \right) x g(x) dx \right|, \quad (4.43)$$

where we use the first estimate in (4.7) and the definition of $\hat{x}(t)$. Applying Jensen inequality and using the estimate

$$\hat{x}(t) \leq e^{-\alpha(\underline{\mathcal{E}} - \bar{\mathcal{E}})} \int_{\mathbb{R}^d} x g(x, t) dx := b_{\underline{\mathcal{E}}} m(t),$$

we get

$$\begin{aligned} \left| \frac{d}{dt} m(t) \right| &= \frac{\nu_F}{M_\alpha(t)} \left| \int_{\mathbb{R}^{2d}} x e^{-\alpha \mathcal{E}(x)} g(x) g(x_*) dx dx_* - \int_{\mathbb{R}^{2d}} x_* e^{-\alpha \mathcal{E}(x_*)} g(x) g(x_*) dx dx_* \right| \\ &= \frac{\nu_F}{M_\alpha(t)} \left| \int_{\mathbb{R}^{2d}} (x - x_*) e^{-\alpha \mathcal{E}(x)} g(x) g(x_*) dx dx_* \right| \\ &\leq \frac{\nu_F}{M_\alpha(t)} \int_{\mathbb{R}^{2d}} |x - x_*| e^{-\alpha \mathcal{E}(x)} g(x) g(x_*) dx dx_* \\ &\leq b_{\underline{\mathcal{E}}} \nu_F \left(\int_{\mathbb{R}^{2d}} |x - x_*|^2 g(x) g(x_*) dx dx_* \right)^{1/2} \\ &= b_{\underline{\mathcal{E}}} \nu_F \sqrt{2} (\rho_0 E_0(t) + \rho_1 E_1(t) - (\rho_0 M_0(t) + \rho_1 M_1(t))^2)^{1/2} \\ &= b_{\underline{\mathcal{E}}} \nu_F \sqrt{2} (V(t) + \rho_0 \rho_1 (M_0 - M_1)^2(t))^{1/2} \rightarrow 0, \quad \text{as } t \rightarrow \infty, \end{aligned} \quad (4.44)$$

since both, $V(t)$ and $(M_0 - M_1)^2(t)$, go to zero as $t \rightarrow \infty$. Thus, there exists $\tilde{x} \in \mathbb{R}^d$ such that

$$\tilde{x} = m(0) + \int_0^t \frac{d}{ds} m(s) ds = \lim_{t \rightarrow \infty} m(t). \quad (4.45)$$

Let us now focus on the term $M_\alpha(t)$

$$\frac{d}{dt} M_\alpha^2(t) = 2M_\alpha(t) \frac{d}{dt} M_\alpha(t) = 2M_\alpha(t) \int_{\mathbb{R}^d} e^{-\alpha \mathcal{E}(x)} \partial_t g(x, t) dx, \quad (4.46)$$

with

$$\begin{aligned} \partial_t g(x, t) &= \partial_t f_0(x, t) + \partial_t f_1(x, t) = \\ &= -\nu_F \nabla_x \cdot \left[(M_1 - x) f_0(x, t) \right] + \frac{\sigma_F^2}{2} \Delta_x \left[D^2(x) f_0(x, t) \right] - \frac{\nu_F}{\rho_1} \nabla_x \cdot \left[(\hat{x}(t) - x) f_1(x, t) \right], \end{aligned} \quad (4.47)$$

where we recall that we assume $\nu_L = \nu_F$ and

$$\sum_{\lambda \in \{0,1\}} \mathcal{T}[f_\lambda](x, t) = 0.$$

We consider the terms separately to obtain

$$\begin{aligned} I_1 &= -\nu_F \int_{\mathbb{R}^d} e^{-\alpha \mathcal{E}(x)} \nabla_x \cdot [(M_1 - x)f_0] dx = \\ &= -\nu_F \alpha \int_{\mathbb{R}^{2d}} e^{-\alpha \mathcal{E}(x)} \nabla \mathcal{E}(x) (x_* - x) df_0 df_1 \geq \\ &\geq -\nu_F \alpha e^{-\alpha \underline{\mathcal{E}}} c_1 \frac{M_\alpha(t)}{M_\alpha(t)} \int_{\mathbb{R}^{2d}} |x_* - x| dg dg_* \geq \\ &\geq -\nu_F \alpha \frac{e^{-2\alpha \underline{\mathcal{E}}}}{M_\alpha(t)} c_1 \left(\int_{\mathbb{R}^{2d}} |x_* - x|^2 dg dg_* \right)^{1/2} \geq \\ &\geq -\nu_F \alpha \frac{e^{-2\alpha \underline{\mathcal{E}}}}{M_\alpha(t)} c_1 \sqrt{2} [V(t) + \rho_0 \rho_1 (M_0 - M_1)^2(t)]^{1/2}, \end{aligned} \tag{4.48}$$

$$\begin{aligned} I_2 &= \frac{\sigma_F^2}{2} \int_{\mathbb{R}^d} e^{-\alpha \mathcal{E}(x)} \Delta_x [D^2(x)f_0] dx = \\ &= -\frac{\sigma_F^2}{2} \alpha \int_{\mathbb{R}^d} e^{-\alpha \mathcal{E}(x)} \Delta \mathcal{E}(x) k |\hat{x}(t) - x|^2 df_0 + \\ &+ \frac{\sigma_F^2}{2} \alpha^2 \int_{\mathbb{R}^{2d}} e^{-\alpha \mathcal{E}(x)} \nabla_x \mathcal{E}(x) \otimes \nabla_x \mathcal{E}(x) k |\hat{x}(t) - x|^2 df_0 \geq \\ &\geq -\frac{\alpha \sigma_F^2}{2} k c_2 e^{-\alpha \underline{\mathcal{E}}} \int_{\mathbb{R}^d} |\hat{x}(t) - x|^2 dg \geq \\ &\geq -\frac{\alpha \sigma_F^2}{2} k c_2 e^{-\alpha \underline{\mathcal{E}}} \int_{\mathbb{R}^{2d}} \int |x_* - x|^2 \frac{e^{-\alpha \mathcal{E}(x_*)}}{M_\alpha(t)} dg dg_* \geq \\ &\geq -\frac{\alpha \sigma_F^2}{2} k c_2 \frac{e^{-2\alpha \underline{\mathcal{E}}}}{M_\alpha(t)} \int_{\mathbb{R}^{2d}} |x_* - x|^2 dg dg_* \\ &\geq -\frac{\alpha \sigma_F^2}{2} k c_2 \frac{e^{-2\alpha \underline{\mathcal{E}}}}{M_\alpha(t)} [V(t) + \rho_0 \rho_1 (M_0 - M_1)^2(t)], \end{aligned} \tag{4.49}$$

and

$$\begin{aligned}
I_3 &= -\frac{\nu_F}{\rho_1} \int_{\mathbb{R}^d} e^{-\alpha \mathcal{E}(x)} \nabla_x \cdot [(\hat{x}(t) - x) f_1] dx \geq \\
&\geq -\frac{\alpha \nu_F}{\rho_1} c_1 e^{-\alpha \mathcal{E}} \int |\hat{x}(t) - x| dg \geq \\
&\geq -\frac{\alpha \nu_F}{\rho_1} c_1 \frac{e^{-2\alpha \mathcal{E}}}{M_\alpha(t)} \left(\int_{\mathbb{R}^{2d}} |x_* - x|^2 dg dg_* \right)^{1/2} \geq \\
&\geq -\frac{\alpha \nu_F}{\rho_1} c_1 \frac{e^{-2\alpha \mathcal{E}}}{M_\alpha(t)} [V(t) + \rho_0 \rho_1 (M_0 - M_1)^2(t)]^{1/2},
\end{aligned} \tag{4.50}$$

where we use assumption (4.37), we integrate by parts, use Jensen inequality and the previous estimates. Altogether, we estimate (4.46) as follows

$$\begin{aligned}
\frac{dM_\alpha(t)}{dt} &\geq -2\alpha e^{-2\alpha \mathcal{E}} \left[c_1 \sqrt{2} \nu_F \left(1 + \frac{1}{\rho_1} \right) (V(t) + \rho_0 \rho_1 (M_0 - M_1)^2(t))^{1/2} + \right. \\
&\quad \left. c_2 \sigma_F^2 k (V(t) + \rho_0 \rho_1 (M_0 - M_1)^2(t)) \right].
\end{aligned} \tag{4.51}$$

Using the estimates for the mean and variance in (4.33)-(4.36) and integrating equation (4.51) we get

$$\begin{aligned}
M_\alpha^2(t) &\geq M_\alpha^2(0) - 2\alpha e^{-\alpha \mathcal{E}} \left[c_1 \sqrt{2} \nu_F \left(1 + \frac{1}{\rho_1} \right) + c_2 \sigma_F^2 k \right] \\
&\quad \cdot \max \left\{ \int_0^t [V(0) + \mathcal{C}_v^0 \gamma_m s] e^{-\mathcal{C}_v s} + \rho_0 \rho_1 \gamma_m e^{-2\nu_F s} ds, \right. \\
&\quad \left. \int_0^t \sqrt{[V(0) + \mathcal{C}_v^0 \gamma_m s] e^{-\mathcal{C}_v s} + \rho_0 \rho_1 \gamma_m e^{-2\nu_F s} ds} \right\}.
\end{aligned} \tag{4.52}$$

We integrate the first integral in (4.52) by parts to get

$$\int_0^t [V(0) + \mathcal{C}_v^0 \gamma_m s] e^{-\mathcal{C}_v s} + \rho_0 \rho_1 \gamma_m e^{-2\nu_F s} ds \leq \frac{V(0)}{\mathcal{C}_v} + \gamma_m \left(\frac{\mathcal{C}_v^0}{\mathcal{C}_v^2} + \frac{\rho_0 \rho_1}{2\nu_F} \right).$$

Moreover, applying Hölder inequality to the second integral in (4.52) yields

$$\begin{aligned}
&\int_0^t \sqrt{[V(0) + \mathcal{C}_v^0 \gamma_m s] e^{-\mathcal{C}_v s} + \rho_0 \rho_1 \gamma_m e^{-2\nu_F s} ds} \leq \\
&\leq \frac{2\sqrt{V(0)}}{\mathcal{C}_v} + \|\sqrt{\mathcal{C}_v^0 \gamma_m s} e^{-\frac{\mathcal{C}_v s}{4}}\|_\infty \int_0^t e^{-\frac{\mathcal{C}_v s}{4}} ds + \frac{\sqrt{\rho_0 \rho_1 \gamma_m}}{\nu_F} \leq \\
&\leq \frac{2\sqrt{V(0)}}{\mathcal{C}_v} + \frac{4\mathcal{C}^*}{\mathcal{C}_v} + \frac{\sqrt{\rho_0 \rho_1 \gamma_m}}{\nu_F},
\end{aligned}$$

where $\mathcal{C}^* := \max_{s \in \mathbb{R}} \sqrt{\mathcal{C}_v^0 \gamma_m s} e^{-\frac{\mathcal{C}_v s}{4}}$ and we use the fact that

$$\sqrt{a+b} \leq \sqrt{a} + \sqrt{b},$$

for and $a, b \geq 0$. Altogether, using assumption (4.38) we obtain

$$M_\alpha^2(t) \geq M_\alpha^2(0) - \mu \geq \frac{1}{4} M_\alpha^2(0), \quad (4.53)$$

with μ defined as in equation (4.40). Thus

$$M_\alpha(t) \geq \frac{1}{2} M_\alpha(0). \quad (4.54)$$

In addition, since $m(t) \rightarrow \tilde{x}$ and $V(t) \rightarrow 0$ as $t \rightarrow \infty$ it holds,

$$M_\alpha(t) = \int_{\mathbb{R}^d} e^{-\alpha \mathcal{E}(x)} g(x) dx \rightarrow e^{-\alpha \mathcal{E}(\tilde{x})}, \quad (4.55)$$

as $t \rightarrow \infty$ as a consequence of Chebishev inequality (see [7]). Thus

$$0 \geq e^{-\alpha \mathcal{E}(\tilde{x})} \geq \frac{1}{2} M_\alpha(0) \iff 0 \geq -\alpha \mathcal{E}(\tilde{x}) \geq \log\left(\frac{M_\alpha(0)}{2}\right), \quad (4.56)$$

that is

$$0 \leq \mathcal{E}(\tilde{x}) \leq -\frac{1}{\alpha} \log(M_\alpha(0)) + \frac{\log(2)}{\alpha}. \quad (4.57)$$

Finally, $0 \leq \mathcal{E}(\tilde{x}) \leq \underline{\mathcal{E}}$ as $\alpha \rightarrow \infty$, since the first term tends to $\underline{\mathcal{E}}$ thanks to Laplace principle and $\log(2)/\alpha$ vanishes in the limit. \square

Remark 5. We emphasize the following observations:

- In order to satisfy condition (4.38), $V(0)$ and $m(0)$ need to be small.
- Note that if we assume to have anisotropic diffusion the convergence is guaranteed independently of the parameters choice and, in particular, of the dimension d . For this reason, all numerical examples of the next section consider the anisotropic noise.

5 Numerical methods

In order to approximate the time evolution of the density $f_\lambda(x, t)$ we sample N_s particles $(x_i^0, \lambda_i^0), i = 1, \dots, N_s$ from the initial distribution. We consider a time interval $[0, T]$ discretized in N_t intervals of length h . The interaction step is solved by means of binary interaction algorithms, see [23, 24] for details.

We denote the approximation of $f_\lambda(x, nh)$ at time t^n by $f_\lambda^n(x)$. For any $\lambda \in \{0, 1\}$ fixed, the next iterate is given by

$$f_\lambda^{n+1}(x) = \left(1 - \frac{h}{\varepsilon}\right) f_\lambda^n(x) + \frac{h}{\varepsilon} \sum_{\lambda_* \in \{0, 1\}} Q_\alpha^+(f_\lambda^n, f_{\lambda_*}^n)(x), \quad (5.1)$$

where $\varepsilon > 0$ is a frequency parameter and $Q^+(f_\lambda^n, f_{\lambda_*}^n)$ is the gain part of the collision operator defined in (3.3). Equation (5.1) can be interpreted as follows: with probability $1 - h/\varepsilon$ an individual in position x does not interact with other individuals and with probability h/ε it interacts with another randomly selected individual. In the following we will assume $h = \varepsilon$.

In order to simulate changes of the label λ , we discretize equation (2.14). For any fixed $x \in \mathbb{R}^d$, we obtain

$$\begin{aligned} f_0^{n+1}(x) &= (1 - \varepsilon \pi_{F \rightarrow L}) f_0^n(x) + \varepsilon \pi_{L \rightarrow F} f_1^n(x), \\ f_1^{n+1}(x) &= (1 - \varepsilon \pi_{L \rightarrow F}) f_1^n(x) + \varepsilon \pi_{F \rightarrow L} f_0^n(x), \end{aligned} \quad (5.2)$$

where $\pi_{F \rightarrow L}(\cdot)$ and $\pi_{L \rightarrow F}(\cdot)$ are the transition rates as defined in (2.10)-(2.13). The details of the numerical scheme are summarized in Algorithm 5.1. Here, the parameters δ_{stall} and j_{stall} are used to check if consensus has been reached in the last j_{stall} iterations within a tolerance δ_{stall} . In more detail, we stop the iteration if the distance of the current and previous mean \hat{x} is smaller than the tolerance δ_{stall} for at least j_{stall} iterations. In this case, the evolution is stopped before the total number of iterations has been reached.

Algorithm 5.1. [GKBO]

1. Draw $(x_i^0, \lambda_i^0)_{i=1, \dots, N_s}$ from the initial distribution $f_\lambda^0(x)$ and set $n = 0$, $j = 0$.
2. Compute \hat{x}^0 as in equation (2.7).
3. **while** $n < N_t$ **and** $j < j_{stall}$
 - (a) **for** $i = 1$ **to** N
 - Select randomly a leader with position y_k^n , $k \neq i$.
 - Compute the new positions

$$\begin{aligned} y_k^{n+1} &= y_k^n + \nu_L \varepsilon (\hat{x}^n - y_k^n) \\ x_i^{n+1} &= x_i^n + \nu_F \varepsilon (y_k^{n+1} - x_i^n) + \sigma_F \sqrt{\varepsilon} D \xi (1 - \lambda_i^n) + \varepsilon \nu_L (\hat{x}^n - x_i^n) \lambda_i^n. \end{aligned} \quad (5.3)$$

- Compute the following probabilities rates

$$p_L = \varepsilon \pi_{F \rightarrow L}(x_i^{n+1}, \lambda_i^n), \quad p_F = \varepsilon \pi_{L \rightarrow F}(x_i^{n+1}, \lambda_i^n).$$

- if $\lambda_i^n = 0$,
with probability p_L agents i becomes a leader: $\lambda_i^{n+1} = 1$.
- if $\lambda_i^n = 1$,
with probability p_F agents i becomes a follower: $\lambda_i^{n+1} = 0$.

end for

(b) Compute \hat{x}^{n+1} as in equation (2.7).

(c) if $\|\hat{x}^{n+1} - \hat{x}^n\|_\infty \leq \delta_{stall}$
 $j \leftarrow j + 1$
end if
 $n \leftarrow n + 1$

end while

The above algorithm is inspired from Nanbu’s method[22], for larger class of direct simulation Monte-Carlo algorithm for interacting particle dynamics we refer to[2, 24].

6 Validation tests

In this section we test the performance of the GKBO algorithm in terms of success rate and number of needed iterations. We consider the translated Rastrigin function with global minimum in $\bar{x} = 1$ for the vast majority of the tests. In the last experiment we compare the results for different benchmark functions (see [16] for a complete list). If not explicitly specified, we run $M = 20$ simulations and, according to [3, 7], we consider a simulation successful if

$$\|\hat{x}(t) - \bar{x}\|_\infty \leq 0.25. \quad (6.1)$$

We set $\alpha = 5 \cdot 10^6$ and we adopt the numerical trick described in [12] to allow for arbitrary large values of α . We assume $N = 200$ and that agents are initially uniformly distributed in the hypercube $[-4.12, 0]^d$, which does not contain the global minimum. At time $t = 0$ we suppose all agents are in the followers status and they change their label according to equation (2.14). For the GKBO algorithm we set the total percentage of leaders is $\rho_1^\infty = 0.5$, if not specified explicitly. Hence, the transition rates are defined as in equation (2.10), with $\pi_{LF} = \pi_{FL} = 0.2$, if the emergence of leaders is random or as defined in equation (2.13) if the labels change according to the weighted criterion defined in Section 2.2. We will consider also a mixed strategy with $\bar{p} = 0.5$, that is, among the total amount of generated leaders, 50% change their labels according to the weighted strategy and the remaining ones change their labels randomly. We let the dynamics in (2.4) to evolve for $N_t = 10000$ iterations with $\varepsilon = 0.1$, where differently specified. We set $j_{stall} = 1000$, $\delta_{stall} = 10^{-4}$. We assume $\nu_F = 1$, $\nu_L = 10$ while the diffusion parameter and the dimension change in the different tests and will be specified later.

6.1 Test 1: Comparison of different followers / leaders ratios

Suppose $\sigma_F = 4$, $d = 20$. Table 1 reports the mean of the number of iterations and success rate (in parenthesis) for the GKBO algorithm tested on the translated Rastrigin function as the leaders mass at the equilibrium ρ_1^∞ , defined as in equation (2.18), varies. The success rate and number of iterations for the KBO algorithm are 1 and 10000 respectively. GKBO outperforms KBO in terms of the number of iterations. However, the success rate of GKBO with random leader emergence deteriorates for $\rho_1^\infty = 0.75$.

	GKBO random	GKBO $\bar{p} = 0.5$	GKBO weighted
$\rho_1^\infty = 0.25$	3008 (1)	3588 (1)	6421 (1)
$\rho_1^\infty = 0.5$	2898 (1)	3477 (1)	6612 (1)
$\rho_1^\infty = 0.75$	4252 (0.6)	4566 (1)	7741 (1)

Table 1: Mean of the number of iterations (success rate) for the GKBO algorithm tested on the translated Rastrigin function as the leaders mass at the equilibrium ρ_1^∞ varies.

6.2 Test 2: GKBO for different choices of \hat{x} .

We compare the results of the algorithm with \hat{x} as in (2.7) and slight modifications given by

$$\hat{x}_F = \frac{\int_{\mathbb{R}^d} x e^{-\alpha \mathcal{E}(x)} f_0(x, t) dx}{\int_{\mathbb{R}^d} e^{-\alpha \mathcal{E}(x)} f_0(x, t) dx}, \quad \text{or} \quad \hat{x}_L = \frac{\int_{\mathbb{R}^d} x e^{-\alpha \mathcal{E}(x)} f_1(x, t) dx}{\int_{\mathbb{R}^d} e^{-\alpha \mathcal{E}(x)} f_1(x, t) dx}, \quad (6.2)$$

which corresponds to the cases where the weighted mean depends only on the followers or only on the leaders, respectively.

In Figure 2 the success rate and number of iterations as σ_F and d varies for \hat{x} (left), \hat{x}_F (middle) and \hat{x}_L (right). In the first row, results for the case with random leaders generation are shown, in the second row the mixed leaders generation with $\bar{p} = 0.5$ and in the third row the case with weighted leaders generation. Note that the performance of the random strategy, especially for large values of the dimension d is higher if $\hat{x}_F(t)$ is used for the estimate of the global minimizer. This can be explained by a better exploration phase of the particles during the evolution, whereas the leaders position \hat{x}_L may result in a less accurate estimate, since labels change randomly. The weighted strategy with $\hat{x}_L(t)$ has computational advantages since leaders are chosen to be the agents with optimal position and the computation of the $\hat{x}_L(t)$ requires a lower number of evaluations of the cost function. This may be advantageous in particular if the evaluation of the cost function is numerically expensive.

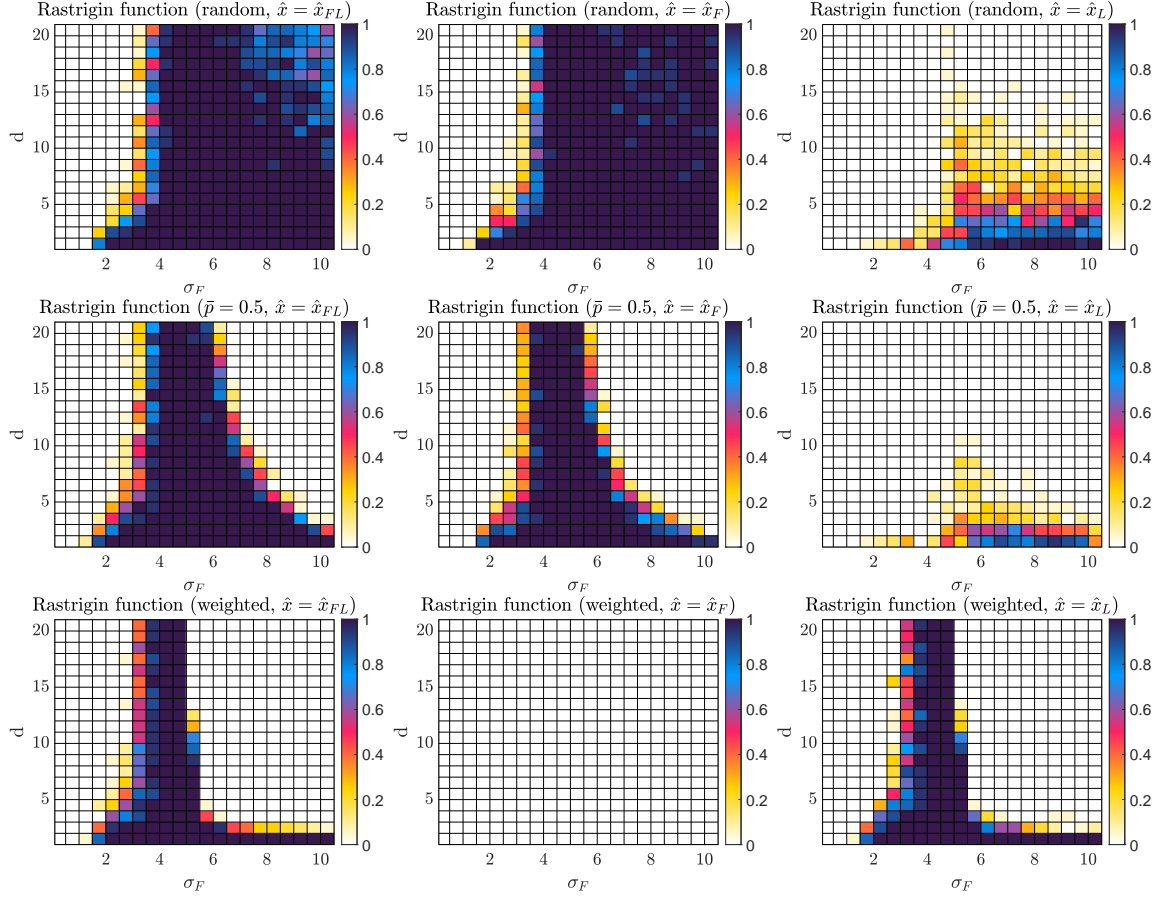


Figure 2: Success rates for varying σ_F and d for the translated Rastrigin function with dynamics simulated with the GKBO method for \hat{x} (left), \hat{x}_F (middle), \hat{x}_L (right). The first row is with random leader emergence, second row with mixed strategy $\bar{p} = 0.5$ and third row with weighted leader emergence.

6.3 Test 3: Comparison in $d = 20$ dimensions for varying σ_F

We fix $d = 20$ and let σ_F vary from $\sigma_F = 0.1$ to $\sigma_F = 10$ to compare the performance of GKBO (equation (2.4)), standard GA (equation (1.2)-(1.3)), the modified GA (equation (1.2)-(1.4)) and the KBO (equation (1.1)).

In Figure 3 the success rates and means of the number of iterations obtained with the different algorithms in the case of the translated Rastrigin function is shown. Here, test GKBO with \hat{x} , \hat{x}_F and \hat{x}_L as defined above and study random leader emergence (left), mixed leader emergence with $\bar{p} = 0.5$ (middle), and weighted leader emergence (right). Although the success rates of KBO and the variants of GKBO behave similar, the GKBO

versions required less iterations. Moreover, we remark that the behavior of the GKBO with weighted leaders generation and with \hat{x} as in equation (2.7) and of the KBO is similar, as expected from our analysis.

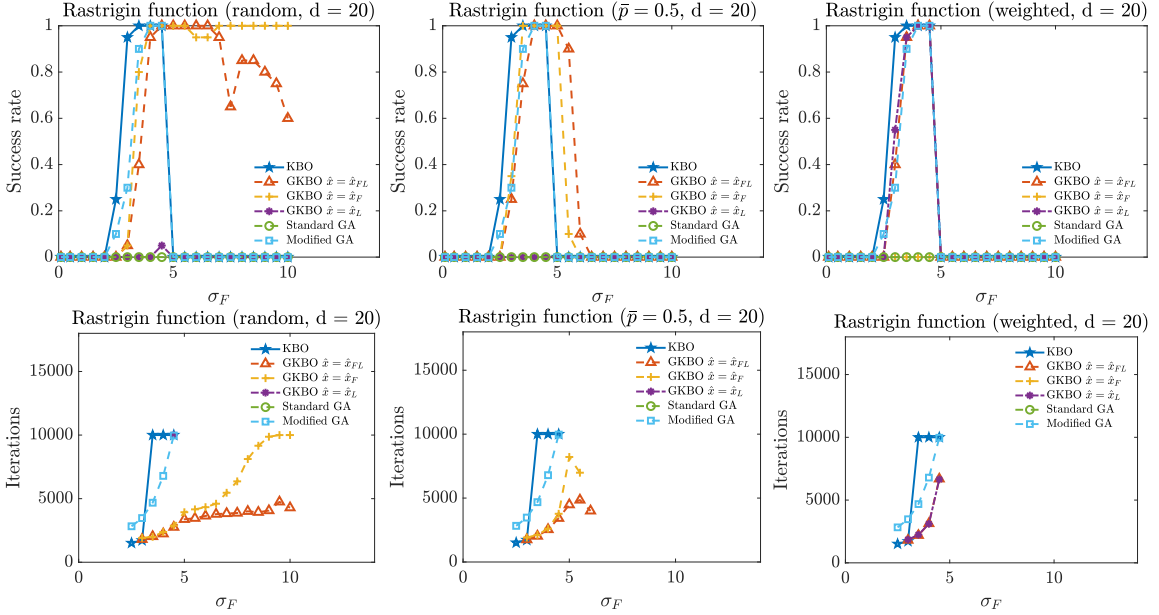


Figure 3: Success rates and means of the number of iterations as σ_F varies and $d = 20$ for the translated Rastrigin function obtained with the different algorithms. On the left leaders emerge randomly, in the, we consider mixed leader emergence with $\bar{p} = 0.5$, and on the right, we have weighted leader emergence. The markers denote the value of the success rates and numbers of iterations for different σ_F .

6.4 Test 4: Comparison of different leader emergence strategies.

Let us fix $d = 20$ and consider the mixed leader emergence strategies as discussed in Remark 2. In Figure 4 on the left we see the success rates for different values of σ_F and \bar{p} , on the right the number of iterations for different values of \bar{p} and for $\sigma_F = 4, 5$. In Figure 5 the success rate and minimum, maximum and mean iterations number for the GKBO method with \hat{x} is shown for $d = 20$ as \bar{p} and σ_F vary.

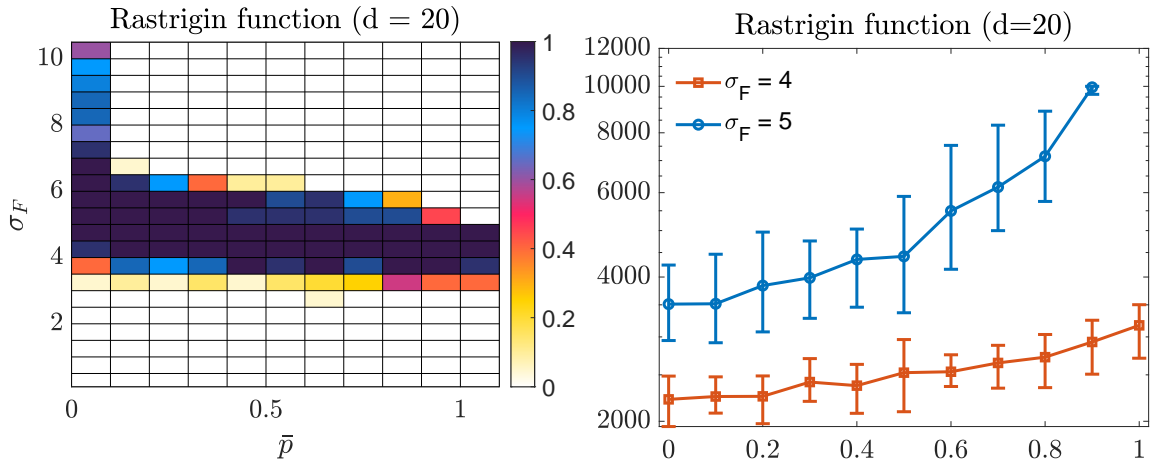


Figure 4: Different leader emergence strategies. On the left, success rates for varying σ_F and \bar{p} and $d = 20$. On the right, max, min and mean number of iterations obtained in the different simulations for $d = 20$ and $\sigma_F = 4, 5$ as \bar{p} varies. The markers denote the number of iterations needed for different \bar{p} and tested on the translated Rastrigin function.

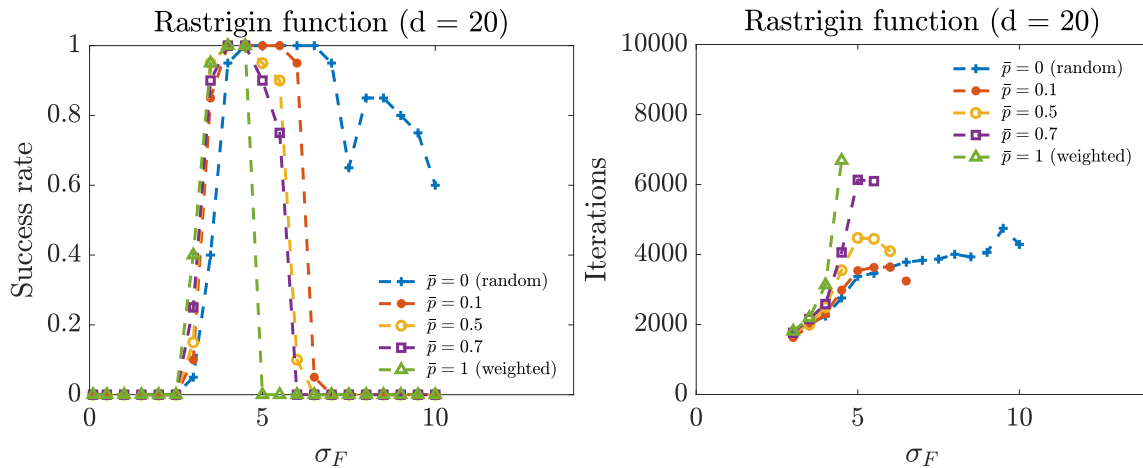


Figure 5: Different leader emergence strategies. Success rates and mean number of iterations for $d = 20$ as σ_F varies and for different values of \bar{p} , tested on the translated Rastrigin function. The markers denote the value of the success rates and number of iterations for different σ_F .

6.5 Test 5: Comparison of different methods for varying d

We fix $\sigma_F = 4$ and vary the dimension d from 1 to 20. Figure 6 shows the success rates and means of the number of iterations of the different methods in the case of the translated Rastrigin function. GKBO uses \hat{x} as in (2.7).

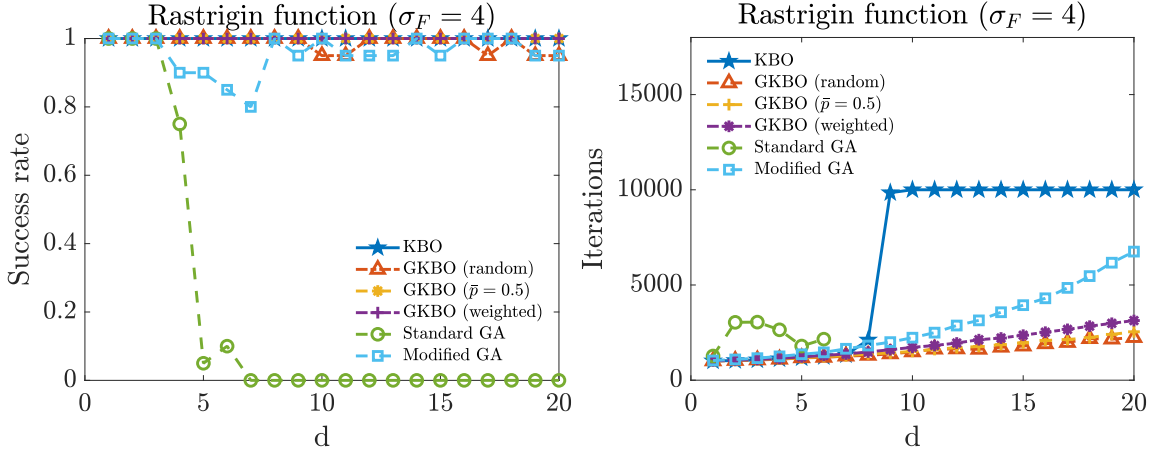


Figure 6: Success rates and number of iterations as d varies for the translated Rastrigin function obtained with the different algorithms. The markers denote the value of the success rates and mean number of iterations.

6.6 Test 6: Comparison of the accuracy for varying frequency ε

Here we study the influence of the frequency parameter ε by comparing the accuracy of the KBO and GKBO with weighted and random leader emergence. We run the test for $M = 100$ simulations assuming the initial data to be normally distributed in the hypercube $[-4.12, 0]^d$, $d = 20$. The accuracy is computed as

$$\|\hat{x}(t) - \bar{x}\|_\infty, \quad (6.3)$$

where \bar{x} is the actual value of the minimum. In Figure 7 the accuracy of the KBO algorithm (left) for GKBO algorithm with random leader emergence (middle) and weighted leader emergence (right) with $\varepsilon = 0.01$ (first row) and $\varepsilon = 0.1$ (second row). Note that in both cases, the values of σ_F for which the method converges with the weighted GKBO and the KBO algorithm is almost the same. If $\varepsilon = 0.01$ the accuracy of the weighted GKBO is higher than the one of the KBO. If $\varepsilon = 0.1$ the random strategy performs better than the other methods since the algorithm converges for almost all the values of σ_F considered. Furthermore, if we look at the case $\sigma_F = 4$, all the methods converge but the random strategy reaches higher levels of accuracy.

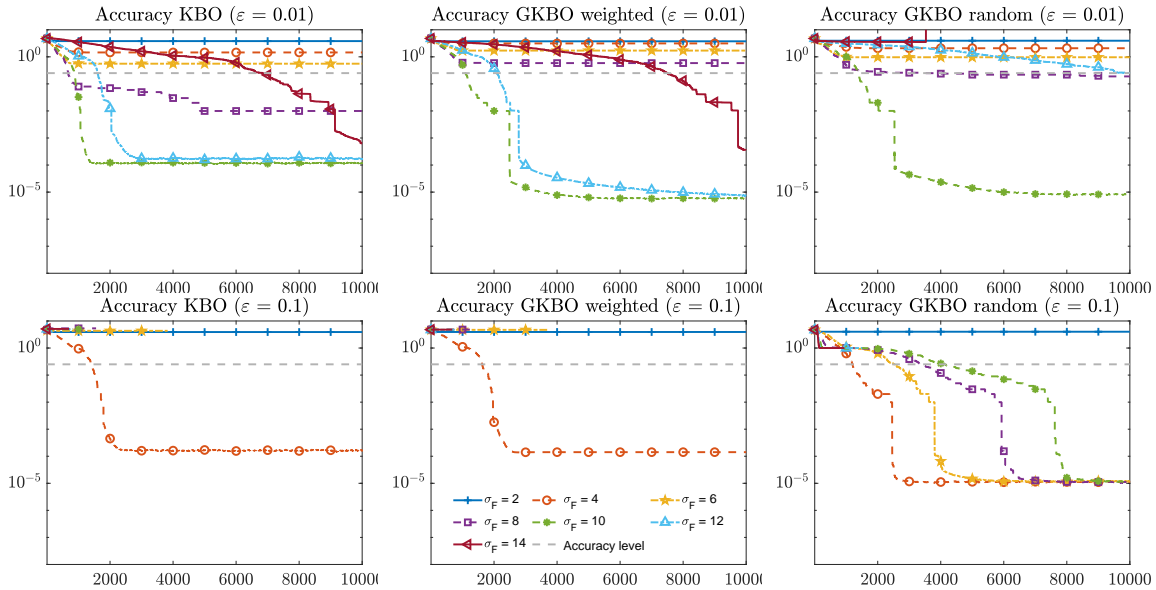


Figure 7: Accuracy of the KBO and of the GKBO algorithm as σ_F varies for $d = 20$ and $\varepsilon = 0.01$ (first row), $\varepsilon = 0.1$ (second row) for the translated Rastrigin function. From the left to the right, KBO, GKBO with random leader emergence and GKBO with weighted leader emergence. The markers have been added to distinguish the lines.

In Figure 8 the results in terms of success rate and number of iterations needed for different values of ε are shown. If $\varepsilon = 0.01$ the success rate of the GKBO methods is smaller than the one of the KBO but the number of needed iterations is reduced. If $\varepsilon = 0.1$, the success rate area is enlarged for the strategy with random leader emergence. With this test we confirm the results obtained in Figure 7. Moreover, the number of iterations is reduced with respect to the KBO and the GKBO method with weighted leader emergence.

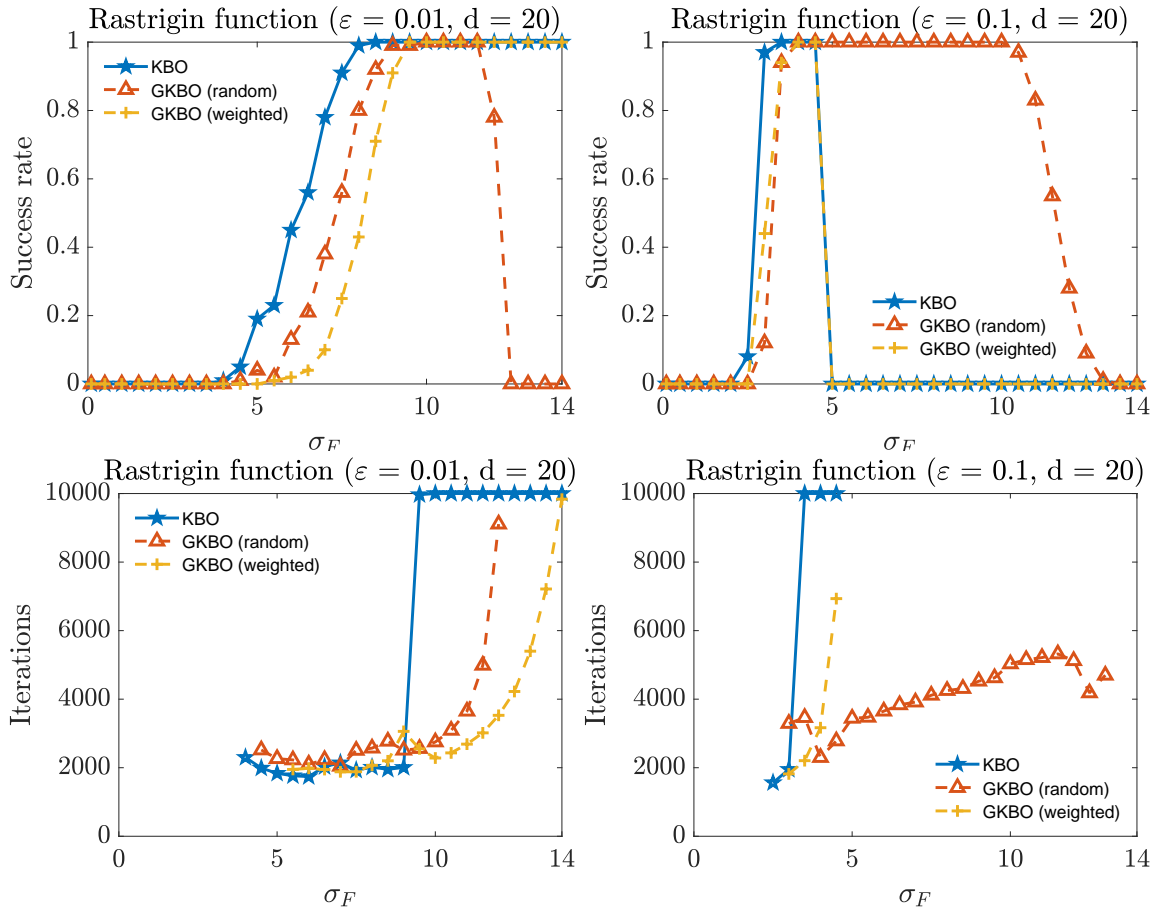


Figure 8: Success rates and means of the number of iterations as σ_F varies for $\varepsilon = 0.01$ (first column), $\varepsilon = 0.1$ (second column) for the translated Rastrigin function. The markers have been added to distinguish the lines.

6.7 Test 7: Comparison of different benchmark functions

In the previous subsection we tested the different algorithms and different parameter sets with the translated Rastrigin function. Now, we choose σ_F such that both the KBO and the GKBO algorithms have success rate equal to one in the previous studies and test different benchmark functions in 20 dimensions. In Figure 9 the comparison of KBO and GKBO in terms of success rate and mean number of iterations are shown. GKBO with both variants of leader emergence outperforms KBO in terms of the number of iterations.

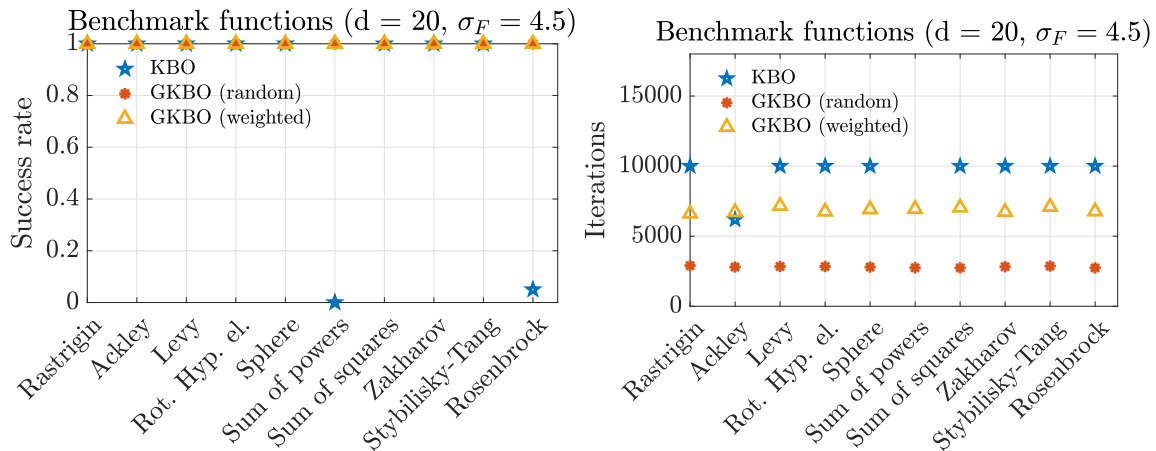


Figure 9: Success rate and mean iterations number for the different benchmark function for fixed $d = 20$ and $\sigma_F = 4.5$. Markers denotes the value of the success rate and of the iterations number for the different benchmark functions.

7 Conclusion

We propose a variant of the KBO method for global optimization which is enhanced by a transition process, inspired by genetic dynamics. These lead to a population divided into two species which we call followers and leaders. We adapt the convergence analysis to the new method and show in particular that the population concentrates in the long-time limit arbitrarily close to the global minimizer of the cost function. Numerical results show the feasibility of the approach and the improvement of the proposed generalization in terms of numerical effort.

Acknowledgments

GA and FF were partially supported by the MIUR-PRIN Project 2022, No. 2022N9BM3N “Efficient numerical schemes and optimal control methods for time-dependent PDEs”.

References

- [1] G. Albi, M. Bongini, F. Rossi, and F. Solombrino. Leader formation with mean-field birth and death models. *Mathematical Models and Methods in Applied Sciences*, 29(04):633–679, 2019.
- [2] G. Albi and L. Pareschi. Binary interaction algorithms for the simulation of flocking and swarming dynamics. *Multiscale Modeling & Simulation*, 11(1):1–29, 2013.

- [3] A. Benfenati, G. Borghi, and L. Pareschi. Binary interaction methods for high dimensional global optimization and machine learning. *Applied Mathematics & Optimization*, 86(1):9, 2022.
- [4] G. Borghi, M. Herty, and L. Pareschi. A consensus-based algorithm for multi-objective optimization and its mean-field description. In *2022 IEEE 61st Conference on Decision and Control (CDC)*, pages 4131–4136. IEEE, 2022.
- [5] G. Borghi, M. Herty, and L. Pareschi. Constrained consensus-based optimization. *SIAM Journal on Optimization*, 33(1):211–236, 2023.
- [6] L. Bottou, F. E. Curtis, and J. Nocedal. Optimization methods for large-scale machine learning. *SIAM review*, 60(2):223–311, 2018.
- [7] J. A. Carrillo, Y.-P. Choi, C. Totzeck, and O. Tse. An analytical framework for consensus-based global optimization method. *Mathematical Models and Methods in Applied Sciences*, 28(06):1037–1066, 2018.
- [8] J. A. Carrillo, S. Jin, L. Li, and Y. Zhu. A consensus-based global optimization method for high dimensional machine learning problems. *ESAIM: Control, Optimisation and Calculus of Variations*, 27:S5, 2021.
- [9] S. Chen, Jingrun Jin and L. Lyu. A consensus-based global optimization method with adaptive momentum estimation. *Communications in Computational Physics*, 31(4):1296–1316, 2022.
- [10] A. Dembo. Zeitouni, O. large deviations techniques and applications. *Applications of Mathematics*, 38, 1998.
- [11] M. Fornasier, H. Huang, L. Pareschi, and P. Sünnen. Consensus-based optimization on hypersurfaces: Well-posedness and mean-field limit. *Mathematical Models and Methods in Applied Sciences*, 30(14):2725–2751, 2020.
- [12] M. Fornasier, H. Huang, L. Pareschi, and P. Sünnen. Consensus-based optimization on the sphere: Convergence to global minimizers and machine learning. *The Journal of Machine Learning Research*, 22(1):10722–10776, 2021.
- [13] D. E. Goldberg. *Genetic algorithms in search, optimization, and machine learning*, volume 1989. 1989.
- [14] S. Grassi and L. Pareschi. From particle swarm optimization to consensus based optimization: stochastic modeling and mean-field limit. *Mathematical Models and Methods in Applied Sciences*, 31(08):1625–1657, 2021.
- [15] J. Haskovec. Flocking dynamics and mean-field limit in the Cucker–Smale-type model with topological interactions. *Physica D: Nonlinear Phenomena*, 261:42–51, 2013.

- [16] M. Jamil and X.-S. Yang. A literature survey of benchmark functions for global optimisation problems. *International Journal of Mathematical Modelling and Numerical Optimisation*, 4(2):150–194, 2013.
- [17] J. Kennedy and R. Eberhart. Particle swarm optimization. In *Proceedings of ICNN'95-international conference on neural networks*, volume 4, pages 1942–1948. IEEE, 1995.
- [18] K. Klamroth, M. Stiglmayr, and C. Totzeck. Consensus-based optimization for multi-objective problems: A multi-swarm approach. *arXiv preprint*, 2022.
- [19] N. Loy and A. Tosin. Boltzmann-type equations for multi-agent systems with label switching. *Kinetic and Related Models*, 14(5):867–894, 2021.
- [20] Z. Michalewicz. *Genetic Algorithms + Data Structures = Evolution Programs*. Springer, 1996.
- [21] M. Mitchell. Genetic algorithms: An overview. *Complexity*, 1(1):31–39, 1995.
- [22] K. Nanbu. Direct simulation scheme derived from the Boltzmann equation. i. mono-component gases. *Journal of the Physical Society of Japan*, 49(5):2042–2049, 1980.
- [23] L. Pareschi and G. Russo. An introduction to Monte Carlo method for the Boltzmann equation. In *ESAIM: Proceedings*, volume 10, pages 35–75. EDP Sciences, 2001.
- [24] L. Pareschi and G. Toscani. *Interacting multiagent systems: kinetic equations and Monte Carlo methods*. OUP Oxford, 2013.
- [25] R. Pinnau, C. Totzeck, O. Tse, and S. Martin. A consensus-based model for global optimization and its mean-field limit. *Mathematical Models and Methods in Applied Sciences*, 27(01):183–204, 2017.
- [26] R. Poli, J. Kennedy, and T. Blackwell. Particle swarm optimization: An overview. *Swarm intelligence*, 1:33–57, 2007.
- [27] C. F. M. Toledo, L. Oliveira, and P. M. França. Global optimization using a genetic algorithm with hierarchically structured population. *Journal of Computational and Applied Mathematics*, 261:341–351, 2014.
- [28] C. Totzeck. Trends in consensus-based optimization. In *Active Particles, Volume 3: Advances in Theory, Models, and Applications*, pages 201–226. Springer, 2021.
- [29] C. Totzeck and M.-T. Wolfram. Consensus-based global optimization with personal best. *Mathematical Biosciences and Engineering*, 17(5):6026–6044, 2020.